Journal of Ceramic Processing Research. Vol. 12, No. 4, pp. 392~397 (2011)

J O U R N A L O F
Ceramic Processing Research

Synthesis and growth of multi-walled carbon nanotubes (MWNTs) by CCVD using Fe-supported zeolite templates

Wei Zhao[a], Hyun Sung Kim[b], Hyung Tae Kim[c], Jianghong Gong[d] and Ik Jin Kim[a,*]

[a]*Institute for Processing and Application of Inorganic Materials (PAIM), Department of Materials Science and Engineering, Hanseo University, 360 Daegok-ri, Haemi-myun, Seosan city, Chungnam, 356-706 Korea*

[b]*Center for Nanomaterials/Korea Center for Artificial Photosynthesis (KCAP), Sogang Bldg., Sogang University, 1-3 Shinsu-dong, Mapo-gu, Seoul, 121-854, Korea*

[c]*Engineering Ceramic Center, Korea Institute of Ceramic Engineering and Technology(KICET), Icheon 467-84, Kyoung-gi do, Korea*

[d]*Department of Materials Science and Engineering, Tsinghua University, Beijing, 100084, China*

Multi-walled carbon nanotubes (MWNTs) were synthesized by catalytic chemical vapor deposition (CCVD) using acetylene as the carbon source and Fe-supported zeolite (FAU) templates. The effect of the catalyst content and the reaction time on the synthesis of CNTs were investigated through transmission electron microscopy (TEM), thermogravimetic (TG) analysis, and Raman spectroscopy. A number of MWNTs synthesized for 1 h had inner and outer tube diameters in the range of 3.8-5.0 nm and 6.3-8.8 nm, respectively, which were smaller than those of conventional thick MWNTs. With increasing iron content in the zeolite, the carbon yield showed a monotonic increasing tendency, reaching 63.1% as the iron content was up to 0.12 mol%. With prolonged reaction times such as 30 minutes, 1 h, 2 h, and 3 h, the inner diameter of the CNTs remained constant while the outer diameter became larger and larger, with the carbon yield after the reaction of 3 h reaching 63.1%.

Key words: Carbon nanotubes, Catalytic chemical vapor deposition, Zeolite, Template, Catalyst.

Introduction

As fascinating novel materials, carbon nanotubes (CNTs) have inspired much interest in the past few years, and intensive research has been performed to identify their remarkable properties [1] and wide range of potential applications as nanoelectronic devices [2] and interconnects [3], sensors and actuators [4], energy storage media [5], and field emitters [6] etc.

CNTs may be viewed as a graphite sheet that is rolled up into a nanometre-scale tubular form (a single-walled carbon nanotube, SWNT) or with additional graphene tubes that form around the core of a SWNT (a multi-walled carbon nanotube, MWNT) [7]. Because the varying degrees of twist of their rolled-up graphene sheets along the length, CNTs can have a variety of chiral structures. Also depending on their diameter and the helicity of the arrangement of graphitic rings in the walls, they have been demonstrated to possess unusual electronic, photonic, magnetic, thermal, and mechanical properties [7]. However, if the price of CNTs still remains as high as it is today (e.g., US$ 500 per gram for SWNT materials-more than 30 times as expensive as gold), any large-scale application of them will be unrealistic. Consequently, a low-temperature, and hence low-cost, synthesis of CNTs with a controllable structure and high purity has become absolutely crucial to the development of the whole field of carbon nanoscience and nanotechnology.

Nowadays, because of enormous potential applications, worldwide effort is being made to produce good-quality CNTs in large quantities by simple and reliable techniques, such as arc-discharge [8], laser evaporation [9] and chemical vapor deposition (CVD) [10]. During the last few years, CVD has been proven to be much more efficient in synthesizing CNTs because of it is a low-cost system, simple operating conditions, easy control of experimental parameters, and feasibility of exploring various carbon sources in solid, liquid and gas forms, although a complete understanding of the growth mechanism of CNTs is still unclear at this time. In particular, catalytic chemical vapor deposition (CCVD) is most frequently employed [11] and offers great advantages over other synthesis methods, where CNTs are grown over catalysts containing nanoparticles of transition metals (Fe, Co, Ni) or related oxides by the decomposition of a carbon source (e.g. CH_4, C_2H_2, C_2H_4, etc.).

In principle, finely dispersed, nanometre-sized metal particle catalysts that preserve their morphology at the CVD processing temperatures are required because controlling the morphology of the catalytic particles during CNT growth strongly affects nanotube characteristics such as thickness, uniformity, and yield. However, as the size of the metal particles decreases to the nanometre scale, they tend to agglomerate. To prevent this, porous materials have

*Corresponding author:
Tel : +82-41-660-1441
Fax: +82-41-660-1402
E-mail: ijkim@hanseo.ac.kr

been proposed as supports. A porous support exhibiting a non-continuous surface and high surface area can not only contribute significantly to particle stabilization and produce a fine dispersion of well-defined particles, but also drastically increase the number of catalytic particles, thus increasing the number of nucleation sites, which are all advantageous to the synthesis of CNTs [12]. Among all the catalytic supports used, zeolites being molecular sieve materials with pore diameters in the range of 3-10 Å have had a significant impact due to their structural homogeneity [13], and high reactive surface area, which makes them excellent host candidates for different types of adsorbing molecules [14] and hence zeolites could be used as supports for catalyst particles to synthesize and grow CNTs.

In the present study, the NaX zeolite (FAU) was used as the template for supporting catalyst nanoparticles to synthesize MWNTs via the CCVD method. Through testing and analysis of the results, the influence of different iron contents supported in the NaX zeolite, and the effect of the reaction time on the synthesis and growth of CNTs were investigated.

Experimental

Preparation of the Fe-supported zeolite catalyst

First, NaX zeolite crystals of 15 μm were synthesized by a hydrothermal method in a mother solution with a composition of 3.5 Na_2O : Al_2O_3 : 2.1 SiO_2 : 1000 H_2O. Second, the synthesized NaX powder (1 g) was refluxed with aqueous solutions of iron(II)-chloride tetrahydrate ($FeCl_2{\cdot}4H_2O$, analytical pure, ≥ 99.0%) by stirring at approximately 30-40 °C for 24 h. The solutions were made by mixing $FeCl_2{\cdot}4H_2O$ powder of different masses (0.04 mol%, 0.08 mol%, and 0.12 mol%) with 250 ml of deionized water. After sufficient stirring, the mixture was further centrifuged, and washed thoroughly with pure ethanol (≥ 99.9%). Ethanol was used here instead of water to prevent the exchanged Fe^{2+} cations from dissolving into the water again. Fe^{2+} was completely ion-exchanged as verified by SEM observations and analysis of the exchanged zeolite samples and by the colorless clear filtrate solution obtained after ion-exchanging. The iron contents in the exchanged zeolite samples were approximately 2.23 wt.%, 4.44 wt.% and 6.72 wt.%. Finally, the powder was dried at ambient temperature and calcined for 3 h at 450 °C in air. According to the iron contents, the three zeolite catalysts were designated as FeNaX0, FeNaX1, and FeNaX2.

Synthesis and growth of CNTs

The CNTs were synthesized by catalytic decomposition of acetylene (C_2H_2) on the calcined Fe-supported NaX zeolite catalysts in a fixed-bed flow reactor at atmospheric pressure. The reactor setup consists of a quartz boat containing the catalyst samples (approx. 100 mg) which were placed in a horizontal electric tubular furnace. The catalysts were gradually heated from room temperature to 700 °C in a nitrogen (N_2) flow (500 sccm) and kept at this temperature for about 15 minutes. Then, a mixture of N_2 (200 sccm) and C_2H_2 (10 sccm) was subsequently fed into the reactor for 1 h, in order for the reaction to proceed. The furnace was then cooled to room temperature under a N_2 flow (500 sccm) and the CNTs produced were collected as a black powder from the quartz boat. According to the catalyst names designated above, the synthesized CNT samples were designated as CNT-FeNaX0, CNT-FeNaX1, and CNT-FeNaX2. Also, according to the same processes described formerly, the sample FeNaX2 mentioned above was selected to synthesize CNTs at 700 °C with a mixture of N_2 (200 sccm) and C_2H_2 (10 sccm) kept feeding for 30 minutes, 1 h, 2 h, and 3 h. All these CNT samples were denoted as CNT30, CNT60, CNT120, and CNT180, respectively.

Characterization

High resolution transmission electron microscopy (HRTEM) observations were carried out on a JEOL JEM-3011 at an accelerating voltage of 200 kV. Samples were prepared by evaporating drops of a zeolite-CNT-ethanol suspension after sonication onto a carbon-coated lacy film supported on a 3-mm-diameter, 300-mesh copper grid.

Thermogravimetric (TG) analysis was performed to measure the amount of carbon deposited in the experiment and also to evaluate the percentage of other forms of carbon. It was conducted under air in a Seiko Extar 7300 (TG/DTA 7300) instrument, with samples of approximately 5 mg heated in air from 25 to 750 °C, at a heating rate of 10 K·minute^{-1}. The Raman spectroscopy measurements were performed with a Raman system FRA-106/S using a laser excitation line at 1064 nm (Nd-YAG) in the range of 200-1800 cm^{-1}.

Result and Discussion

TEM results

Fig. 1(a), (b) and (c) show the TEM image of the well-formed NaX zeolite crystal and its schematic structure, and the TEM image of the catalyst sample FeNaX2, respectively. Fig. 1(a) reveals a high degree of structural order in the crystal surface formed inside the complementary pores between two distinct peaks, each centered at 13.942 Å, corresponding to the inner diameter of the zeolite structure. As shown in Fig. 1(b), NaX zeolite can be described as an

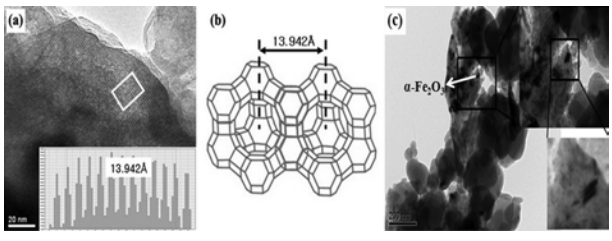

Fig. 1. (a) TEM image of the synthesized NaX zeolite nanocrystal, (b) the schematic structure of the NaX zeolite, and (c) TEM image of the catalyst sample FeNaX2.

ensemble of sodalite cages or β-cages joined hexagonal prisms. Generally, this structure can be envisaged as a stack of layers of sodalite cages joined by double six rings (D6R) in a tetrahedral arrangement like the carbon atom in diamond, with a center of inversion at the center of the D6R. The β-cage is surrounded by an even larger cage, the supercage (a cavity with a diameter of about 13 Å), which forms a three-dimensional network with each cage connected tetrahedrally to four other supercages through the 12-membered ring opening with a crystallographic aperture of 7-8 Å [15]. In the present study, this nano-structured zeolite material was applied as the host material for holding catalyst nanoparticles in order to synthesize CNTs [16].

After ion-exchanging and calcination, catalyst nanoparticles (small black spots in Fig. 1(c)) randomly dispersed on the external surface of the catalyst sample FeNaX2 are clearly evident, and their main component was confirmed to be α-Fe_2O_3 by XRD (already shown previously in [17], and not shown here), even though its content was too low to be easily observed. Even after the synthesis of the CNTs, these catalyst nanoparticles still remain in CNTs, as shown by the black spot inside CNTs in Fig. 2.

According to a previous study [18], ambigurity still remains on what is the exact catalyst for the synthesis of CNTs. Moreover, the breakdown of the zeolitic structure after the calcination of Fe^{2+}-exchanged NaX zeolite can be readily identified in Fig. 1(c) where the zeolite crystal has been ruptured, containing irregularly shaped cavities with a size distribution in the range of mesopores.

Fig. 2 shows CNT synthesis mechanisms as well as typical TEM images for them. Some isolated CNTs (Fig. 2(a)) point to the so-called base-growth model, while some of them (Fig. 2(b)) point to the tip-growth model of CNTs in our CCVD process. Meanwhile, due to the powder state of the catalysts used in our study, combined with the existing base- and tip-growth models, CNTs can be grown from catalyst particles along both directions at the same time, the schematic of which is shown in Fig. 2(c).

As reported in our previous study [17], all synthesized CNTs clearly are MWNTs. The inner and outer diameters of quite a number of them are largely distributed in the range of 3.8-5.0 nm, and 6.3-8.8 nm, respectively, with an interlayer distance of 0.25-0.45 nm, indicating that some are thinner than graphite (typically 0.34 nm in interlayer spacing) [19]. Therefore, these observations suggest that probable diameters of the synthesized CNTs were below 10 nm, which are much smaller than those synthesized by a conventional CVD method. This is the first reason why the catalyst sample FeNaX2 was selected for following reactions for different times. Also, CNTs could be synthesized at a lower iron content, exhibiting a growth (including length and yield) tendency with increasing iron content. This suggests that more catalyst particles act as "seeds" for the CNT synthesis with increasing iron content, leading to the increasing CNT yield, which can obviously be obtained from the data shown in Table 1. This is the second reason for choosing the catalyst sample FeNaX2 for following CNT synthesis for different reaction times.

Table 1. Carbon yield (TGA) and quality (Raman spectroscopy) of synthesized CNTs (CNT- FeNaX0, CNT-FeNaX1, and CNT-FeNaX2; CNT30, CNT60, CNT120, and CNT180)

Catalyst sample		Carbon yield %	Raman ratio (I_D/I_G)
CNT-FeNaX0		47.7	0.89
CNT-FeNaX1		54.8	0.83
CNT-FeNaX2	CNT30	45.3	0.89
	CNT60	63.1	1.20
	CNT120	46.0	0.59
	CNT180	63.1	0.85

Following, the effect of synthesizing time on CNT products was investigated by keeping constant the reaction temperature (700 °C) and the catalyst sample (FeNaX2). HRTEM images in Fig. 3(a)-(d) show four series of synthesized CNTs, CNT30, CNT60, CNT120, and CNT180, respectively. Since all these images are not specially selected, they all are considered reasonable. Through a comparison from Fig. 3(a) to 3(d), it is easy to find that CNT30, CNT60, CNT120, and CNT180 are MWNTs, which have inner diameters close to 10 nm without distinct changes between them. However, their outer diameters have a monotonic increase with prolonging reaction time, which represents the thickening of the CNT walls, corresponding to the increasing number of layers of CNT walls, that is, 15, 19, 20, and 25 layers. This result reveals that carbon atoms decomposed from C_2H_2 form coaxial cylindrical graphene sheets layer by layer around the core of CNTs with a prolonging reaction time.

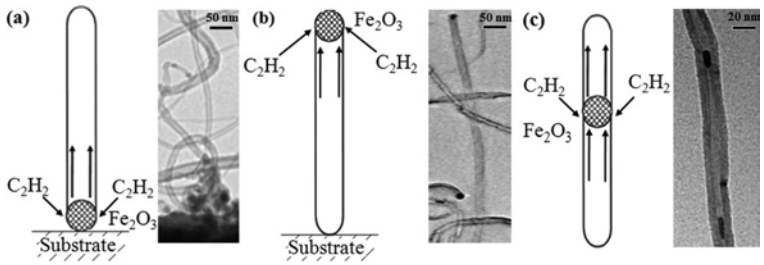

Fig. 2. CNT synthesis mechanisms: (a) base-growth model, (b) tip-growth model, and (c) combination of base- and tip-growth model.

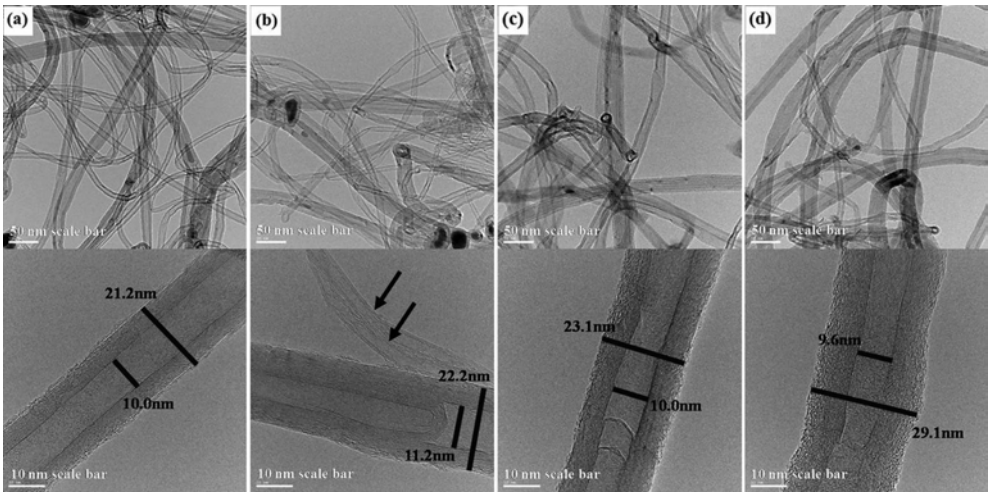

Fig. 3. HRTEM images of CNTs synthesized for different reaction times CNT30, (b) CNT60, (c) CNT120, and (d) CNT180.

Despite the increasing tendency, it is obvious that CNTs catalyzed by FeNaX2 for 1 h (CNT60) have inhomogeneity. Of them some are much thicker with the inner diameter being approximate 11.2 nm and walls of up to 19 layers and an end-capped CNT inside, without any catalyst nanoparticles at their ends, and some are small-sized bundles, only containing a few walls of approximate 3-5 layers (pointed by arrows), as shown in Fig. 3(b). This may result from inhomogeneous catalyst particles caused by the rupture of the zeolite. Therefore, the synthetic conditions need modification in order to obtain well-formed MWNTs with thin walls and a narrow inner diameter distribution.

TG results

Fig. 4 shows the TG curves of NaX zeolite, FeNaX2, and CNT samples CNT-FeNaX0, CNT-FeNaX1, and CNT-FeNaX2. Generally, the decomposition of C_2H_2 on metal ion-supported catalysts using the CCVD method leads to the formation of a mixture of CNTs and amorphous carbon on the catalyst surface.

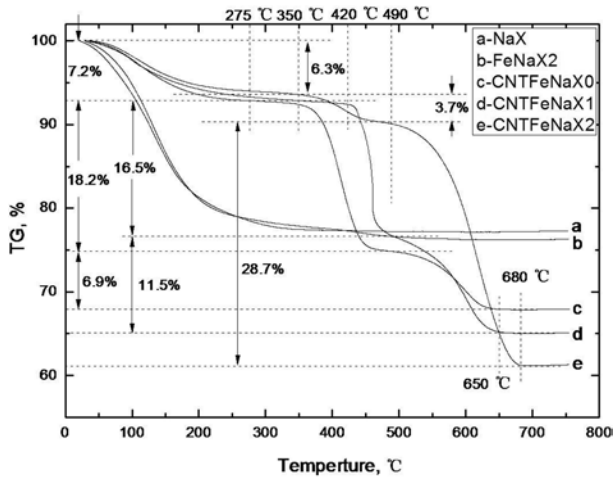

Fig. 4. TG curves of (a) NaX zeolite, (b) FeNaX2, (c) CNT-FeNaX0, (d) CNT-FeNaX1, and (e) CNT-FeNaX2.

As shown in Fig. 4, the initial weight loss (up to 275 °C) for both a and b samples is attributed to the loss of physically absorbed water in the zeolite. However, TG curves c, d and e reveal an initial weight loss until 275 °C, which are all much less than that of both a and b. This may be caused by the elimination of most of the water inside the ion-exchanged zeolite during the CNT synthesis. After that, all the CNTs undergo a two-step combustion process which begins at temperatures of $\geqslant$ 350 °C depending on the nature of the carbon species [20]. The first step (350-490 °C) corresponds to the combustion of the amorphous carbon species, and the second ($\geqslant$ 500 °C) corresponds to the combustion of MWNTs. Interestingly, both c and d samples had a much larger weight loss (18.2% and 16.5%, respectively) which is identified as the first-step combustion of the amorphous carbon species than that of sample e (3.7%). In addition, Fig. 4 also indicates that three samples c, d and e exhibit a gradually increasing weight loss (6.9%, 11.5% and 28.7%, respectively) at the second combustion step, which represents the loss of synthesized MWNTs with increasing iron contents suppoted in the zeolite. Both the monotonic decreasing weight loss in the first-step combustion and the increasing weight loss in the second-step combustion imply that more iron content suppoted in the NaX zeolite template means less amorphous carbon yield and more CNT production. When the temperature is higher than 680 °C, the residual weight gradually decreases with increasing iron content suppoted in the NaX zeolite template.

To summarize, the burning temperature (~490 °C) of the MWNTs in our study was a little higher than that of SWCNTs (~480 °C) [21] but much lower than that of the generally thick MWNTs (~700 °C) grown by CVD method [22].

Next, Fig. 5 shows the TG curves of CNT samples, CNT30, CNT60, CNT120, and CNT180. All of them present a similar three-step weight loss process, which comprises an initial loss of physically absorbed water in the zeolite, the first-step combustion of amorphous carbon species, and the second-step combustion of synthesized

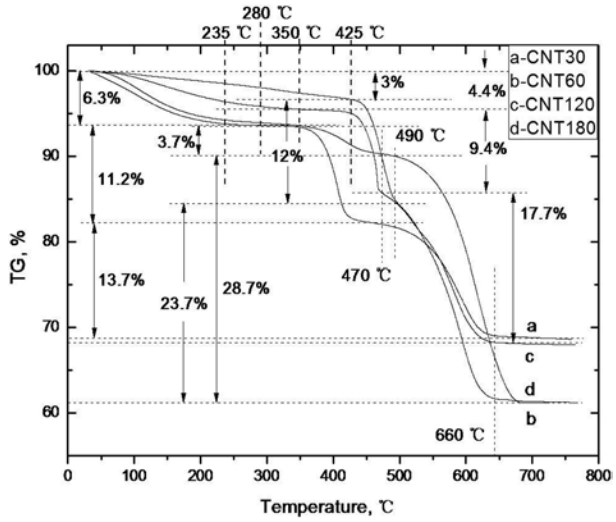

Fig. 5. TG curves of CNTs synthesized for different reaction time (a) CNT30, (b) CNT60, (c) CNT120, and (d) CNT180.

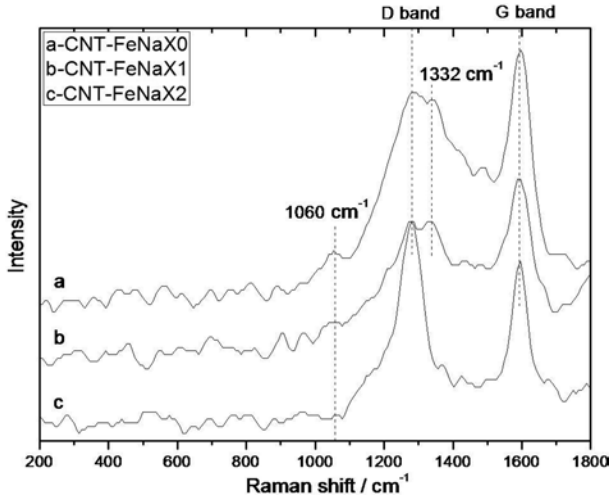

Fig. 6. Raman spectra of CNTs synthesized by different contents of Fe-supported NaX zeolite (a) CNT-FeNaX0, (b) CNT-FeNaX1, and (c) CNT-FeNaX2.

MWNTs. The initial loss of physically absorbed water in CNTs synthesized for 30 minutes, 1 h, 2 h, and 3 h, which should have been the same, is 6.3%, 6.3%, 4.4%, and 3%, respectively. This difference may be generated from the natural error caused by using catalysts prepared in different batches despite using the same method. Also the weight loss of their amorphous carbon species is 11.2%, 3.7%, 9.4%, and 12.0%, respectively; that of their MWNTs is 13.7%, 28.7%, 17.7%, and 23.7%, respectively. In general, all these values show a decreasing trend of the formation of amorphous carbon species and an increasing trend of the MWNT yield, which are in accordance with the analysis of TEM images shown in Fig. 3.

The usual method to estimate the quantity of the deposited carbon during decomposition of small hydrocarbon molecules on metal ion-containing catalysts by CCVD is calculated as follows:

$$\text{Carbon yield (\%)} = (m_{tot} - m_{cat})/m_{cat} \times 100\% \qquad (1)$$

where m_{cat} is the initial amount of the catalyst (before the reaction) and m_{tot} is the total weight of the sample after the reaction. The use of TG data allows for the determination of the deposited carbon. The results for the synthesized CNTs by different contents of Fe-supported NaX zeolite and by the catalyst sample FeNaX2 for different reaction times are given in Table 1.

Raman spectra

Fig. 6 shows the Raman spectra of the synthesized CNTs observed under Nd-YAG laser of wavelength 1064 nm (excitation energy 2.41 eV) at 110 mW power.

In all spectra for the CNT samples CNT-FeNaX0, CNT-FeNaX1, and CNT-FeNaX2, there are two characteristic peaks around the wavelengths 1280 cm^{-1} and 1590 cm^{-1}, which are identified as D- and G-bands, respectively. The G-band represents the tangential stretching (E_{2g}) mode of graphite and is related to the vibration of sp^2-bonded carbon atoms in a two-dimensional hexagonal lattice; the D-band is associated with the disordered, sp^3-hybridized carbon present as impurities and dispersive defects in the graphitic sheets [23]. Here, close to the D-peak of samples a and b, there is a side peak at approximately 1332 cm^{-1}, which is seen in a previous study [24] as the diamond sp^3 peak, and does not exist in the spectrum of sample c. In addition, a broad peak at around 1060 cm^{-1} (T peak) is shown in a and b much higher than in c, which represents the amorphous carbon [25]. This result is in accordance with the TG analysis in section 3.2.

The relative intensity ratios of the D- to G-bands (shown in Table 1) reveal the degree of disorder in the graphite sheets and they can be used as a measure of the crystallinity of the synthesized CNTs. The ratios in our study were similar to those reported in the literature (0.7-1.3) for MWNTs conventionally synthesized by CCVD [26]. It is clear that the CNT sample CNT-FeNaX1 has a much higher crystallinity than the other two catalysts. As shown in Fig. 6, the relatively weak G-mode and strong D-mode of sample c indicate that the synthesized MWNTs have poor structural ordering and a high concentration of defects, although the HRTEM images presented in Fig. 3 show the clear graphite layer structure.

Fig. 7 shows the Raman spectra of CNTs synthesized for different reaction times. In the range of 200-1800 cm^{-1}, D- and G-bands for CNT samples CNT30, CNT60, CNT120, and CNT180 are shown around the wavelength of 1280 cm^{-1} and 1590 cm^{-1}, respectively. Also the relative intensity ratios of the D- to G-bands are shown in Table 1, with the CNTs synthesized for 2 h having the lowest value, indicating that they have the highest crystallinity. Despite that, Fig. 7 shows a broad D peak for CNT30, CNT60, and CNT180, which indicates the existence of defective graphitic layers on the wall surfaces, like diamond at approximately 1332 cm^{-1} [24]. Also, there are some small

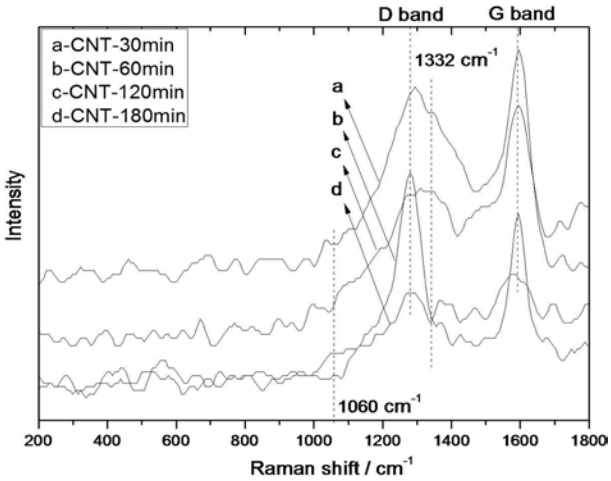

Fig. 7. Raman spectra of synthesized CNTs by catalyst FeNaX2 for different reaction Times CNT30, (b) CNT60, (c) CNT120, and (d) CNT180.

and complex bumps in the spectra for CNT30, CNT60, and CNT180 around the wavelength 1060 cm^{-1} which are identified in the study [25] as amorphous carbon, which is in accordance with the analysis given above.

Note that, except for a sudden increase at 1 h, the intensity of the D peak decreases with prolonged reaction time, indicating that the defect content has an ensemble decreasing tendency even though it is unexpectedly larger when the reaction proceeds for 1 h; the G peak stops keeping single and sharp until the reaction is carried out for 3 h, when it becomes broader and shorter and also has a side peak, indicating that the CNTs obtained after a much longer reaction time may have a weaker crystallinity.

Conclusions

MWNTs were synthesized by CCVD using Fe-supported NaX zeolite as the catalyst. After a reaction of 1 h, quite a number of CNTs had inner and outer diameters in the range of 3.8-5.0 nm and 6.3-8.8 nm, respectively. With an increasing iron content in the NaX zeolite, the carbon yield shows a monotonic increasing tendency, reaching 63.1% when the iron content is up to 6.72 wt.%. In addition, with prolonged reaction times such as 30 minutes, 1 h, 2 h, and 3 h, the inner diameter of the CNTs remained constant while the outer diameter became larger and larger, with the carbon yield after the reaction of 3 h reaching 63.1%. This allows the NaX zeolite to be a container for catalysts and as a guide template for MWNT growth. All CNTs showed two apparent peaks at the wavelengths 1280 cm^{-1} and 1590 cm^{-1}, which were identified as D- and G-bands, respectively. The CNTs obtained after a much longer reaction time may have a weaker crystallinity.

Acknowledgement

This research was supported by the National Research Foundation of Korea (NRF) grant funded by the Korea government (MEST) and by a grant from the 2010 Fundamental R&D Program of Hanseo University, Korea.

References

1. C. Yu, L. Shi, Z. Yao, D. Li and A. Majumdar, Nano Lett. 5 (2005) 1842-1846.
2. M. Fuhrer, H. Park and P.L. McEuen, IEEE Trans, Nanao-technol. 1 (2002) 78-85.
3. J. Li, Q. Ye, A. Cassell, H.T. Ng, R. Stevens and J. Han, Appl. Phys. Lett. 82 (2003) 2491-2493
4. R.H. Baughman, C.X. Cui, A.A. Zakhidov, Z. Iqbal, J.N. Barisci and G.M. Spinks, Science 284 (1999) 1340-1.
5. C. Liu, Y.Y. Fan, M. Liu, H.T. Cong, H.M. Cheng and M.S. Dresselhaus, Science 286 (1999) 1127-1129.
6. C. Liu, Y. Tong, H.M. Cheng, D. Golberg and Y. Bando, Appl. Phys. Lettl. 86 (2005) 223114(1-2).
7. P.J.F. Harris, Cambridge University Press, Cambridge, (2001).
8. T.W. Ebbesen and P.M. Ajayan, Nature 358 (1992) 220-222.
9. A. Thess, R. Lee, P. Nikolaev, H. Dai, P. Petit, J. Robert, C. Xu, Y.H. Lee, S.G. Kim, A.G. Rinzler, D.T. Colbert, G.E. Scuseria, D. Tomanek, J.E. Fischer and R.E. Smalley, Science 273 (1996) 483-487.
10. M. Endo, K. Takeuchi, K. Kobori, K. Takahashi, H.W. Kroto and A. Sarkar, Carbon 33[7] (1995) 873-881.
11. K.P. De Jong and J.W. Geus, Catal. Rev.-Sci. Eng. 42 (2000) 481-510.
12. H. Ago, S. Imamura, T. Okazaki, T. Saitoj, M. Yumura, and M. Tsuji, J. Phys. Chem. B 109 (2005) 10035-10041.
13. I.J. Kim and H.J. Lee, Key Eng. Mater. 280-283 (2005) 891-894.
14. M. Karthik, A. Vinu, A.K. Tripathi, N.M. Gupta, M. Palanichamy and V. Murugesan, Micropor. Mesopor. Mater. 70 (2004) 15.
15. H.J. Lee, Y.M. Kim, O.S. Kweon and I.J. Kim, Journal of the European Ceramic Society 27 (2007) 561-564.
16. G.L. Che, B.B. Lakshmi, E.R. Fisher and C.R. Martin, Nature 393[6683] (1998) 346-349.
17. W. Zhao, D.N. Seo, H.T. Kim and I.J. Kim, Journal of the Ceramic Society of Japan 118[11] (2010) 983-988.
18. S. Esconjauregui, M. Caroline, Whelan and K. Maex, Carbon 47 (2009) 659-669.
19. S. Iijima, Nature 354[6348] (1991) 56-58.
20. C.M. Chen, M. Chen, F.C. Leu, S.Y. Hsu, S.C. Wang, S.C. Shi and C. F. Chen, Diamond Relat. Mater. 13 (2004) 1182-1186.
21. I.W. Chiang, B.E. Brinson, A.Y. Huang, P.A. Willis, M.J. Bronikowski, J.L. Margrave, R.E. Smalley and R.H. Hauge, J. Phys. Chem. B 105 (2001) 8297-8301.
22. C.J. Lee, J.H. Park, Y. Huh and J.Y. Lee, Chem. Phys. Lett. 343 (1999) 33-38.
23. L.D. Shao, G. Tobias, C.G. Salzmann, B. Ballesteros, S.Y. Hong, A. Crossley, B.G. Davis and M.L.H. Green, Chem. Commun. (2007) 5090-5092.
24. A.C. Ferrari, J. Robertson, Phys. Rev. B 63 (2001) 121405(1-4).
25. A.C. Ferrari, J. Robertson, Phys. Rev. B 64 (2001) 075414 (1-13).
26. K. Kwok and W.K.S. Chiu, Carbon 43 (2005) 437-446.